

THE SUPERCONDUCTING SEPARATED-ORBIT CYCLOTRON TRITRON

U. Trinks

Physik Department, Technische Universität München,
D-8046 Garching, Germany

ABSTRACT

The Tritron will be a separated-orbit cyclotron with superconducting channel magnets and superconducting accelerating cavities. All magnets and cavities are manufactured, the assemblage is going on. The Tritron design is expected to overcome the focusing problems and current limitations of other types of cyclotrons. It seems to be a promising candidate for providing high cw-currents of protons and heavy ions up to specific energies of ≈ 600 MeV/u at rather low cost.

1. THE TRITRON DESIGN

The Tritron project is a study of a new type of cyclotron, a superconducting separated-orbit cyclotron with a MP-tandem as injector.^{1,2)} A separated-orbit cyclotron was proposed first by F.M. Russell.^{3,4)} The Tritron shall increase the ion energies by a factor of 5. The beam is

guided by 238 superferric, independently adjustable channel magnets with alternating gradients along a spiral orbit with almost 20 turns. The spiral consists of 30° -arcs and drift lengths between them. The turn separation outside the channel magnets is $\Delta r = 4$ cm. Radially neighbouring channels are joined into 12 flat sectors (see Fig.1). In each second of the intermediate free sectors a superconducting rf-cavity with fixed frequency $\nu_{rf} = 170$ MHz provides for the rather strong accelerating voltage corresponding to the turn separation. In the remaining intermediate sectors beam position probes for both transverse coordinates are installed to control the current setting of the channel magnets, when centering the beam along the spiral orbit.

The specific feature of the Tritron design is the strong transversal and longitudinal focusing.^{5,6)} The betatron oscillation numbers can be chosen far from the stability limits, resonances can be avoided. Longitudinal focusing is caused by the fact, that the magnetic field will

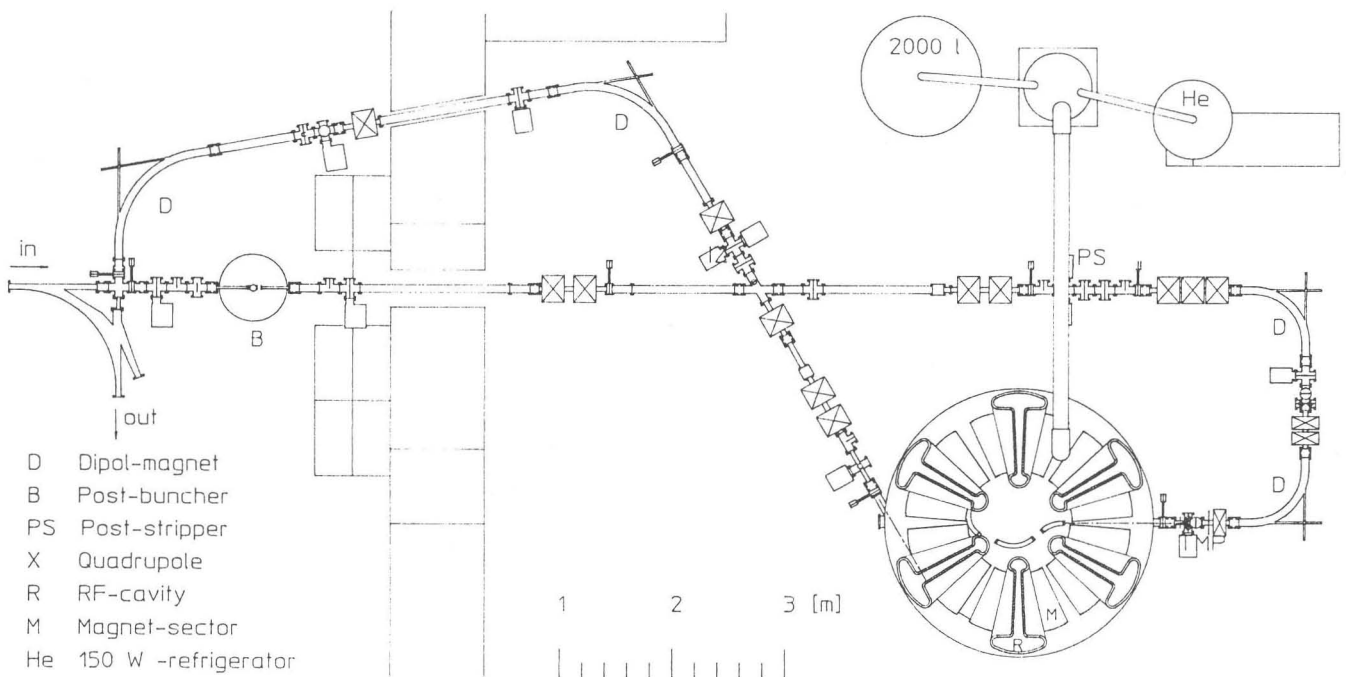


Fig. 1. Plan view of the Tritron hall.

not be isochronous for non-central particles. The relative variation of the revolution frequency $\Delta\nu/\nu_o$ is given by the variation of the velocity and of the mean orbit radius r (turn length over 2π):

$$\frac{\Delta\nu}{\nu_o} = \frac{\Delta v}{v_o} - \frac{\Delta r}{r} \quad (1)$$

$\nu_o = \nu_{rf}/h$ with the harmonic number h is a subharmonic of the fixed rf-frequency. v_o is the velocity of the isochronous particle running along the orbit, that is with $\Delta r = 0$ and $\Delta v = 0$. If the field levels of all channel magnets are adjusted properly, the central particle in the bunch will move with $\Delta r = 0$. However the energy of the central particle may differ from the isochronous energy, so that $\Delta v \neq 0$. Then the resulting frequency deviation $\Delta\nu$ will lead to stationary coherent energy and phase oscillations of the whole bunch with respect to a particle moving isochronously, if the slope of the accelerating voltage as function of the phase is positive. The oscillation numbers are approximately $Q_{coh} \simeq 0.3$ per turn. Noncentral particles with $\Delta r \neq 0$ will execute incoherent synchrotron oscillations with respect to the centre of the bunch. Due to the difference concerning the Δr -term in Eq.1 the oscillation numbers Q_{inc} are about $0.7 \cdot Q_{coh}$.

The beam centering procedure starts at the first position probe. Here the beam is assumed to be centered already, however with a horizontal angle error of the beam axis, which will not be measured by the probes. Then the currents in both succeeding channel magnets will be changed equally, until the beam is centered at the next position probe, too. If the first channel is radially focusing (positive gradient) and the second radially defocusing (negative gradient), then the angle error will be reduced automatically, as shown in Fig.2.

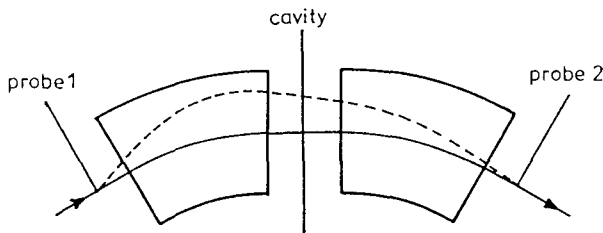


Fig. 2. Centering the beam at probe 2 causes a reduction of angle error, if the first magnet has radially increasing and the second decreasing field.

The injection is made simply by three superconducting channel magnets. The third one imposes the bending limit for the Tritron, because it has the smallest bending radius with $\varrho_{inj} = 30$ cm, compared to $\varrho_1 = 43$ cm for the channel magnets on the first turn. For extraction no element is needed at all. In principle several rings of the Tritron type with increasing radii could be combined to achieve specific energies of the ions of several 100 MeV/u.

All main components of the Tritron were new developments with uncertain results. Therefore the final en-

ergy was chosen to be rather moderate: e.g. for protons a maximum energy of $\simeq 43$ MeV corresponding to an maximum accelerating voltage of $\simeq 0.53$ MV per cavity was planned. In the meantime all cavities and channel magnets are manufactured (except the first two of three injection magnets) and partly tested with much better results than expected originally. Best values so far for the unloaded quality factor Q_o , for the maximum voltage U_{max} , and for the maximum gap field E_{gap} in the cavities are: $Q_o = 1.9 \cdot 10^9$, $U_{max} = 1.2$ MV and $E_{gap} = 10.6$ MV/m. The maximum current in the main coils of the channel magnets, achieved without any training, was 2000 A (design value 1450 A). Thus the magnetic induction can be as high as $B_{max} \simeq 1.9$ T in the sector channels respectively $\simeq 2.4$ T in the third injection channel, which was made from FeCo. Due to these encouraging test results maximum energies of $\simeq 74$ MeV for protons respectively $\simeq 6$ MeV/u for the very heavy ions may be obtained, provided that the terminal voltage of the tandem is at least $\simeq 15$ MV.

The fixed rf-frequency causes the revolution frequency $\nu_o = \nu_{rf}/h$ as well as the final energy T_2 to have discrete values. Due to the longitudinal focusing harmonic numbers h ranging from $\simeq 14$ to $\simeq 55$ can be used. In the upper right quarter of Fig.3 the corresponding energy levels T_2 are shown as horizontal bars with h as parameter. The density of the levels increases strongly with growing values of h . By the choice of the initial energy and rf-phase a distinct stationary coherent energy oscillation will be stimulated, so that the final energy can be varied somewhat (yet $\Delta r = 0$ for the centre of the bunch!). Thus the gaps between neighbouring levels can be filled partially (not shown in Fig.3). While the right ends of the bars are meaningless, the left ends give (on the horizontal axis) the effective accelerating voltage $Q/A \cdot U_{max}$ needed at least per cavity, according to:

$$\frac{Q}{A} U_{max} = T_o \beta^2 \gamma^3 \frac{\Delta r}{r_2} \cdot \frac{1}{T_{rans}} \quad (2)$$

Here Q/A and T_o are the specific charge and rest energy. β and γ correspond to T_2 at the mean extraction radius $r = r_2 = 1.45$ m. T_{rans} is the transittime factor. Neglecting T_{rans} , from Eq.2 follows $Q/A \cdot U_{max} \sim T_2$ in non-relativistic approximation. For small values of h the linear dependence is apparent. At high numbers h the decreasing transittime factor requires higher accelerating voltages.

In the upper left quarter of Fig.3 the final energy is plotted versus the injection energy T_1 :

$$T_2 = \frac{\gamma_2}{\gamma_1} \left(\frac{r_2}{r_1} \right)^2 T_1 \quad (3)$$

In non-relativistic approximation this again has a linear dependence: with $r_1 = 0.66$ m follows $T_2 \simeq 4.9 T_1$.

In the lower left quarter of Fig.3 the specific charge (vertical axis) is given, which is needed to bend the ions with the energy T_1 along the third injection channel,

either with $B_{inj} = 2.4$ T or 2.0 T (bending limit), according to

$$T_1 = \sqrt{\left(\frac{Q}{A}\right)^2 (e \cdot c \cdot \varrho_{inj} \cdot B_{inj})^2 + T_o^2} - T_o \quad (4)$$

In non-relativistic approximation T_1 is proportional to $(Q/A)^2 \cdot B_{inj}^2$. In the lower right quarter of Fig.3 the effective accelerating voltage is shown for given Q/A and cavity voltage U_{max} .

Figure 3 demonstrates the limits imposed on the different types of particles. Protons with $Q/A = 1$ could be injected by $B_{inj} < 2.4$ T without problems for all harmonic numbers $h \geq 11$, however the limitation of the cavity voltage U_{max} will lift the minimum h to $h = 14$ corresponding to $U_{max} = 0.81$ MV and $T_2 = 74.7$ MeV. Light ions with $Q/A = 0.5$ would need $B_{max} > 2.4$ T for $h \leq 20$, the bending limit sets the minimum to $h = 21$ corresponding to $T_2 = 31.2$ MeV/u and a cavity voltage of at least $U_{max} = 0.77$ MV. Energies near to the Coulomb barrier of about 5.5 MeV/u can be obtained for $h \approx 49$ with $Q/A \cdot U_{max} = 0.16$ MV. The injection energy would be $T_1 = 1.16$ MeV/u. Due to the very low yield of ions with specific charge $Q/A \geq 0.215$ for ^{238}U , ^{208}Pb or even ^{198}Au at this low energy, the induction $B_{max} = 2.4$ T in the injection channel is of crucial importance for the very heavy ions, which are of special interest for physics. The accelerating voltage in the cavities then has to be $U_{max} \geq 0.73$ MV.

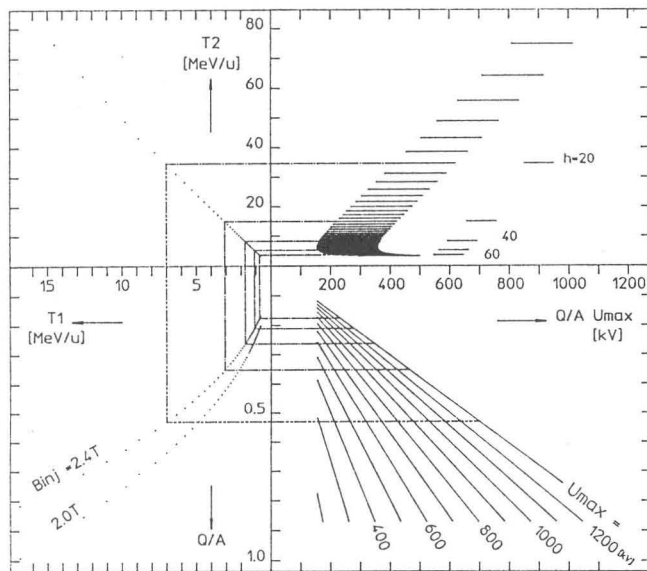


Fig. 3. Characteristics of the Tritron. Explanations see text.

2. THE MAGNETS

The channel magnets are of the window-frame type with the coils bent up and down at the ends (Fig.4).⁷⁾ The entrance and exit edges are not tilted. The bending radius of the innermost channels is $\varrho_1 = 43$ cm.

It increases from turn to turn by $\Delta\varrho = 26.94$ mm. All sectors (sector angle 20°) are of equal geometrical shape except the last two, where one channel is removed for injection respectively extraction. Cooling is made indirectly by cooling pipes (thermal siphon). Each sector

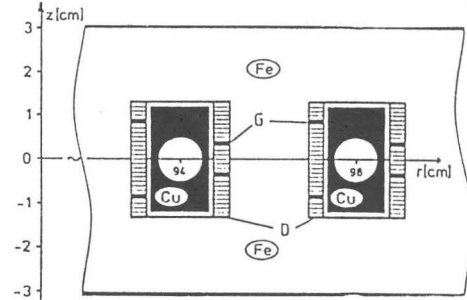


Fig. 4. Cross section through a magnet sector with two adjacent channels. G gradient windings, D insulating layers.

consists of two steel sheets (Fe with 1.8% Si), each 30 mm thick, with curved slots every 4 cm (width 22 mm, depth 15.5 mm). All pieces from steel are Ni plated to avoid rust. The maximum induction is limited by the saturation of the steel to about $B_{sat} \approx 2$ T. Thus the overall current density in the superconducting coils can be chosen ≥ 600 A/mm², and the radial width of the coil can be made small (≈ 3 mm). The coils consist of 2×13 windings (including a separate gradient winding in each half-coil) of a Rutherford-type cable (0.69×2.88 mm², 14 strands, each diam. 0.4 mm and 54 filaments, Cu/Nb = 1.4, 2 insulating layers of glass cloth with prepreg, each 0.1 mm thick). The half-coils were wound directly into the slots by a computer controlled winding machine (640 half-coils within 17 months) and then vacuum impregnated with epoxy in situ. A copper profile (with a 11 mm bore for the beam) shields the coil from beam losses. Flat disc springs between the copper profile and the coil prevent the coil from cracking. The total effective width of the coils and the walls of the shield is 9 mm. So one gets for the maximum radial geometrical aperture a_x :

$$a_x = \frac{\Delta r}{1 + \frac{B_{max}}{B_{sat}}} - 9 \text{ mm} \quad (5)$$

The normalized field gradients are $\frac{\partial B}{\partial \varrho} \cdot \frac{1}{B} = 3.6 \text{ m}^{-1}$ in the radially and -4.9 m^{-1} in the axially focusing channels, if the gradient windings are operated without current: $I_g = 0$. The field indices $n = \frac{\partial B}{\partial \varrho} \cdot \frac{\varrho}{B}$ increase linearly with the turn number (see Fig. 5). The betatron oscillation numbers range from $Q_x \approx 1.3$ to 1.6 and $Q_y \approx 0.8$ to 1.7 for $I_g = 0$. Axial misalignments of the magnet sectors with a first harmonic amplitude of 0.3 mm would cause a strong increase of the axial betatron amplitudes at the $Q_y = 1$ resonance. To shift the field indices of the 10 innermost turns upward, the corresponding channels could be operated with a current $I_g \neq 0$, opposite to the current

in the main coils. In order to correct even non-resonant axial deflections from misalignments, small superconducting magnets ($\int B\delta s \leq 5 \cdot 10^{-3} \text{ Tm}$) with radially directed fields will be inserted into the six intermediate sector gaps in front of the position probes. The distribution of

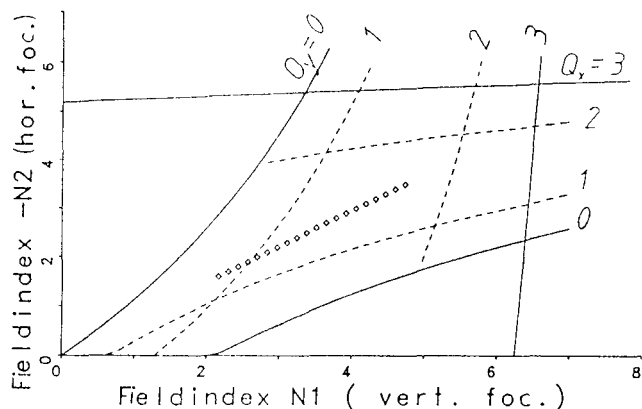


Fig. 5. The field indices n_1 and n_2 .

the cables in the coil cross section should be as uniform as possible to avoid disturbing field terms of higher order than the linear one from the gradients. Quadratic contributions of $|\frac{\Delta B}{B}| > 5 \cdot 10^{-3}$ at $x = \pm 4 \text{ mm}$ apart from the central orbit would cause the dynamic aperture to be less than the geometrical. Negative quadratic contributions at the ends of the coils, where both half-coils spread apart, can be compensated by positive terms introduced by proper choice of the distance of the gradient windings from the central plane of symmetry and by additional insulating layers between the half-coils and the ground of the slots in the steel ($\approx 0.5 \text{ mm}$). Field measurements showed, that the relative quadratic contributions, averaged along the channels, stay below $1.5 \cdot 10^{-3}$ at $x = \pm 4 \text{ mm}$ for $I_g = 0$.

The local magnetic field inside the superconducting coil induce persistent screening currents in those filaments, which are not yet occupied by a transport current. The resulting dipol fields depend on the present and previous current settings and cause the gradient to depend on the current too. Above $\approx 500 \text{ A}$, the variations of the gradients by these magnetization effects were measured to be less than 5%. The effect on the quadratic field contributions is negligible. These results are in agreement to those obtained from a computer model calculation.

In order to guide the beam along the central orbit the current of each of the 238 channels has to be adjusted individually. The difference between maximum and minimum current of all channels is less than $\approx 170 \text{ A}$. All main coils will be connected in series. Each half of a main coil has a superconducting switch with superconducting contacts in parallel, which will be turned to the superconducting state as soon as the appropriate current of the coil is achieved. Further variation of the current from the power supply will be shared between the switch

and the coil, according to the ratio of the inductances. The switches are made of superconducting wires (hairpin shape) with the copper matrix etched off along $\approx 3 \text{ cm}$, which can be heated above the critical temperature with an Allen-Bradley resistor. The filaments at the ends of the switch are mixed with those of all strands of the coil cable and pressed within a copper tube (pressure $\approx 5 \cdot 10^4 \text{ N/cm}^2$) to form the superconducting contacts.

From voltage measurements across a complete sector and across individual channels the inductances of the channels were determined to range from 1 to $3 \cdot 10^{-4} \text{ H}$ in agreement with values calculated from the field energy. The mean inductance of the 40 superconducting switches was $2.6 \cdot 10^{-7} \text{ H}$. From this one expects a current variation in the main coils of some 10^{-3} of the variation of the switch current. Indeed a relative change of the field of $< 6 \cdot 10^{-4}$ in channel 19 e.g. was observed, when the main current in channel 18 was lowered from 1000 A to 850 A , while the switches of all other channels (including that of channel 19) were superconducting. If the main current of several neighbouring channels was changed simultaneously, the field variation in the channel with the switch superconducting was larger, indicating an increased 'cross talking'. This effect will not set in, when the beam is thread through succeeding channels, because then the main current of only one channel per sector will be changed.

The rate of current change in the superconducting switches could be as high as 20 A/sec without quenches for currents in the switches below 220 A . At a rate of 0.5 A/sec no switch quenched below 310 A . The total resistance of all normal conducting joints between adjacent coils was less than $2.7 \cdot 10^{-7} \Omega$ corresponding to a mean value less than $7 \cdot 10^{-9} \Omega$ per joint. The total dissipated heat in the joints would be less than 1 W per sector at the maximum current of 1800 A .

When energizing all channels at the same time, extended eddy current loops are induced in the steel, which are linked to all channels and which decay with a time constant of the order of several minutes. If only one channel is energized while the flux is kept constant in all others by the superconducting switches, then no long lasting eddy currents are observed.

3. THE CAVITIES

The six rf-cavities with a radial length of 120 cm are of the reentrant type with radially prolonged accelerating lips, forming a wedge-shaped gap of 62 mm length at the first beam hole and 128 mm at the last, see Fig.6. The accelerating lips are $\approx 90 \text{ cm}$ long and $\approx 15 \text{ cm}$ high. The surrounding bulge for the magnetic rf-flux was chosen as big as possible to keep the surface fields and thus the losses small. All radii of curvature were made sufficiently large to get the electrical peak field not more than 1.5 of the maximum field in the gap. The beam hole diameters are 13 mm , the length of the cutoff bores in the accelerating lips is 30 mm . The radial field and voltage characteristics are shown in Fig.7. The radial

increase of the voltage due to that of the gap length corresponds approximately to the requested curve according to Eq.2 (β and γ according to $r_1 \leq r \leq r_2$). So far a maximum voltage $U_{20} = 1.2$ MV was obtained at the last beam hole corresponding to a maximum electrical gap field at the 13th hole of 10.6 MV/m and a maximum surface induction of ≈ 0.023 T near the first beam hole.

The cavities are operated in the fundamental mode at

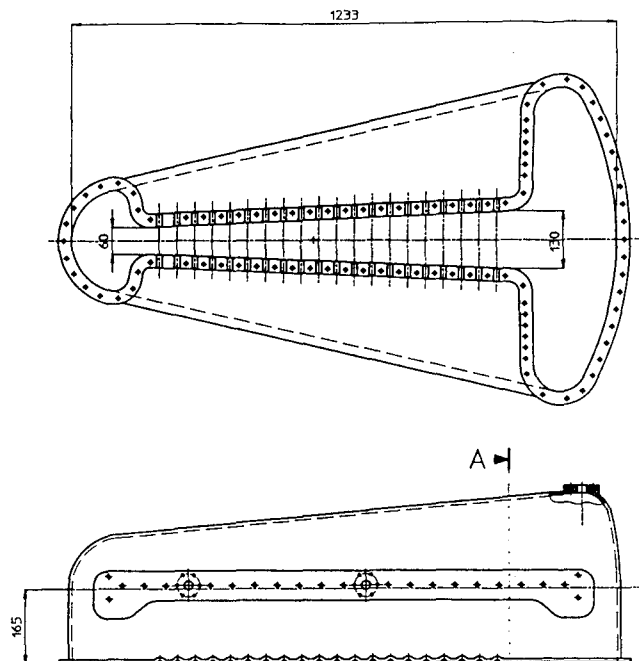


Fig. 6. Cross sections of the upper half of a cavity. Numbers in mm.

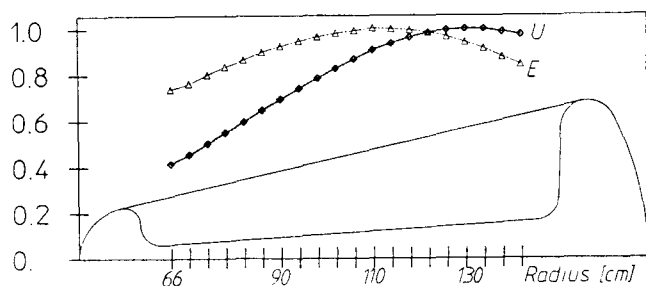


Fig. 7. The radial characteristics of the normalized voltage U and gap field E .

a frequency of $\nu_{rf} = 170$ MHz. No currents should cross the horizontal plane of symmetry. Therefore the cavities can be made from two halves, which are connected simply by a flat joint. The cavity halves were fabricated by electroplating copper (for the most parts 10 mm thick) onto fibre-glass shells, which were removed afterwards.⁹⁾ The copper halves were electroplated with a $\approx 5\mu\text{m}$ thick layer of PbSn (4 Sn, 96 Pb atoms), which has a critical temperature of $T_c = 7.5$ K. Two O-shaped

cooling pipes are attached on both sides of the cavity. During a test more than 100 W dissipated rf-power were removed without quenching the cavity.

Due to rather small mechanical tolerances the frequencies of the cavities are equal within $\pm 3 \cdot 10^{-4}$. Tuning is made in three steps: coarse (20 kHz) by mechanical deformation (at the arrow in Fig.6), fine (300 Hz) by moving sapphire rods into the rf-field volume, and final phase corrections by a fast electronic control system adapted from the S-DALINAC.¹⁰⁾ Sapphire has a low rf-loss factor and high thermal conductivity at low temperature. The frequency shift due to electromagnetic pressure was -230 Hz at a maximum voltage $U_{20} = 1200$ kV at the last beam hole. Frequency variations due to acoustic vibrations are less than 10 Hz, partially owing to the fact, that the cavities are supported very near to the nodes of the fundamental vibration (frequency: ≈ 170 Hz).

PbSn is a better superconductor than pure Pb because of its enhanced stability against chemical reactions, the lower BCS resistance and better throwing power during the electroplating procedure.¹¹⁾ The temperature dependent part of the surface resistance is given by

$$R_{BCS} = 6.85 \cdot 10^{-5} \nu^{1.9} \cdot \frac{1}{T} e^{-\frac{15.1}{T}} \quad (6)$$

with R_{BCS} in Ω , ν in GHz and T in K. Due to the rather low frequency of 170 MHz the cavity needs not to be cooled down below 5 K. At $T = 5$ K one has $R_{BCS} = 2.3 \cdot 10^{-8} \Omega$, which gives the unloaded quality factor $Q_0 = G / R_{BCS} = 4.1 \cdot 10^9$, where $G = 95 \Omega$ is the geometry factor of the cavity. This Q_0 -value represents an upper limit. Additional contributions R_{RES} to the surface resistance R_S , which are independent from temperature, e.g. dielectric layers, normal-conducting spots or magnetic flux causing persistent currents will lower the Q_0 -value. The stray fields of the channel magnets and current leads have to be shielded by thin steel sheets below $\approx 10^{-4}$ T.

In Fig.8 some measurements of the Q_0 -values versus U_{20} respectively the maximum gap field E_{max} at the 13th beam hole are shown. The temperature was below 5 K, the background induction $\leq 8 \cdot 10^{-5}$ T. The cavities were electroplated with the PbSn-layers in alphabetical order. The improvement of the later Q -values indicates the progress in the surface preparation technique. The curves slope at low voltages slightly, at those above ≈ 600 kV more steeply due to starting field emission. The dotted curves are for constant dissipated heat, 6 W respectively 12 W per cavity. The broken line gives the limiting value mentioned above. The best measurements are not far from this limit. Up to now the quality factor showed no degradation during several months, though the cavities were exposed to air each time, when the vacuum vessel was opened. The insulating vacuum is not separated from the beam vacuum in the Tritron. This good results in spite of the large total surface of ≈ 3 m² per cavity can be explained by the fact, that the heat, dissipated in small normal-conducting spots e.g., will be led

away from the thin PbSn layer into the copper body very effectively, causing a rather small temperature increase and preventing the spot to grow, at least below a certain maximum power input. In addition the skin depth of the rf-fields in normal-conducting PbSn exceeds the thickness of the layer considerably.

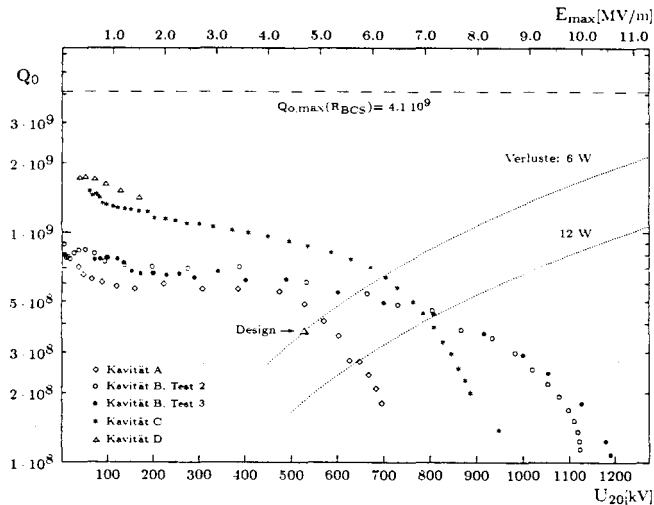


Fig. 8. Unloaded quality factor Q_0 versus the voltage U_{20} resp. the maximum gap field.

4. PRESENT STATUS

The assemblage of all parts inside the vacuum vessel is going on. The cryosystem including the refrigerator (150 W at 4.6 K) is operating well. Evacuation of the vessel needs about 24 h. Cooling down from 300 K to 4.2 K was accomplished within 50 h with somewhat reduced refrigerator power, up to now with $\approx 40\%$ of the final mass (≈ 6 tn). The beam guiding system between the tandem and the Tritron is ready except the post-buncher¹³⁾, which is under test. The computer control system of the tandem and Tritron is in an advanced state. First beam entering the Tritron is expected at the end of this year.

5. FUTURE DEVELOPMENTS

The Tritron development was started to overcome the limitations of the conventional cyclotron on the energy due to transverse resonance and focusing problems, and on the beam intensity due to the missing longitudinal focusing and the extraction problems. The maximum proton current of the 590 MeV - ring cyclotron at the Paul Scherrer Institute in Villigen/Switzerland is expected to be 1.5 mA.¹⁴⁾ With cyclotrons of the Tritron type proton energies as high as 1 GeV and currents comparable to those in linacs (≥ 100 mA) appear to be attainable in principle. A 500 MeV proton beam with a current of 10 mA, that is a beam power of 5 MW, would give a spallation neutron source with a thermal

neutron flux of 10^{15} n/(cm²sec), which is comparable to the highest flux from a nuclear reactor (at the Institute Laue Langevin in Grenoble). While the flux from a reactor hardly can be increased much above this value due to cooling problems in the core (power density ≈ 3 MW/l), the power density in the target of a 500 MeV spallation source would allow currents of more than 100 mA. Of special interest on the long-term will be the possibility to produce energy by fission without the safety problems of nuclear plants, avoiding radioactive waste with long lifetimes by transmutation. For this purpose superconductivity improves the efficiency considerably. Of course, there will be many steps in the development of high intensity Tritron rings before, therefore the following design considerations are restricted to a proton current of 10 mA.

A system of two Tritron rings will be investigated. The extraction radius of the first shall be equal to the injection radius of the second ring: $r_{ex}^I = r_{in}^{II}$. The total beam losses shall not exceed 10 W or 10^{-8} in relative units to avoid quenching of the superconducting elements as well as high activation levels. Then the geometrical aperture $a_{x,y}$ should be at least 10 standard deviations $\sigma_{x,y}$, assuming a gaussian particle density. With the turn separation $\Delta r = 10$ cm, $B_{max} = 1.75$ T and $B_{sat} = 1.9$ T one gets from Eq.5 $a_x = 43$ mm (LAMPF: 19.1 mm, PSI-injection cyclotron: $a_y = 35$ mm).

All cavities are assumed to be equal and about twice as large as the present Tritron cavities. Larger cavities with a weight of ≥ 3 tn would be difficult to handle and to produce with the present electroforming technique. The accelerating gap length shall range from 20 cm at the first and 40 cm at the last beam hole. 16 beam holes with a radial distance of 150 cm from the first to the last are planned. The accelerating lips are vaulted asymmetrically with respect to the radial axis, so that one flat magnet sector could be installed in the concave side without losing space at a most dense packing of the cavities along the ring, as shown in Fig.9. The cut-off bores in the accelerating lips with a diameter of 43 mm will have a length of 120 mm. The overall length of the cavities will be about 3 m, the frequency in the fundamental mode is estimated to be $\nu_{rf} \approx 90$ MHz. At the last beam hole a maximum voltage $U_{16} = 2$ MV is assumed, corresponding to a field in the gap $E_{16} = 5$ MV/m respectively a maximum gap field $E_{max} = 5.8$ MV/m near the 10th beam hole. The dissipated heat in the cavity walls is given by

$$P_w = 2\pi \cdot \nu_{rf} \cdot E_{cav} \cdot \frac{R_s}{G} \quad (7)$$

Here E_{cav} is the electromagnetic energy stored in the cavity, and $R_s = R_{BCS} + R_{RES}$ is the surface resistance. The dissipated heat in the existent Tritron cavities is about $P_w \approx 6$ W at a field level of $E_{max} \approx 5.8$ MV/m (see Fig.8). The dissipated heat in the walls of a new cavity is estimated to be at most about $P_w = 36$ W, assuming for ν_{rf}/G about one half and for E_{cav} about 12

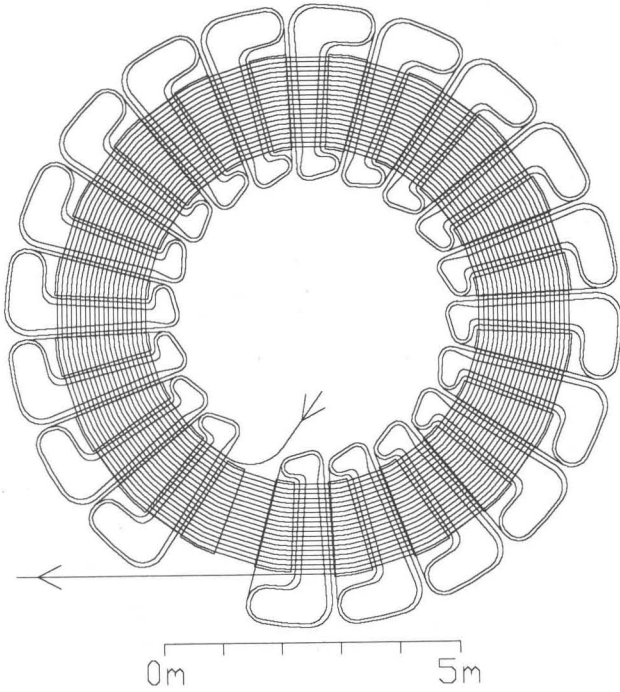


Fig. 9. Schematic plan view of a large Tritron ring for 500 MeV protons.

times the value of the old cavities. R_s is assumed to stay constant.

The mean orbit radius at extraction is given by

$$r_{16} = \varrho + \frac{N_{sec} (l_{gap} + 2d_{rift})}{2\pi} \quad (8)$$

with the bending radius

$$\varrho = \frac{m_o \cdot c}{e} \cdot \frac{\beta \cdot \gamma}{B_{max}} \quad (9)$$

$l_{gap} = 40$ cm is the length of the accelerating gap at the 16th beam hole. $d_{rift} = 18$ cm is the drift length between the effective edges of the accelerating gap and the succeeding channel magnet.

$$N_{sec} = f \cdot \frac{U^*}{U_{16}} \quad (10)$$

is the minimum number of sectors, with $U_{16} = 2$ MV, and U^* according to Eq.2 ($Q/A = 1$ for protons and $T_{rans} = 1$). The factor $f \simeq 1.15$ takes into account, that some overvoltage is needed for accelerating at a phase below $\pi/2$, and that the cavity of one sector will be omitted to leave space for the injection channel. Combining Eq.2,8,9, and Eq.10 gives r_{16} as function of γ at extraction

$$r_{16} = \sqrt{\gamma^2 - 1} \frac{m_o \cdot c}{2e \cdot B_{max}} \cdot \left\{ 1 + \sqrt{1 + \frac{2e \cdot f}{\pi \cdot m_o \cdot U_{16}} (l_{gap} + 2d_{rift}) \cdot B_{max}^2 \cdot \Delta r \cdot \gamma} \right\} \quad (11)$$

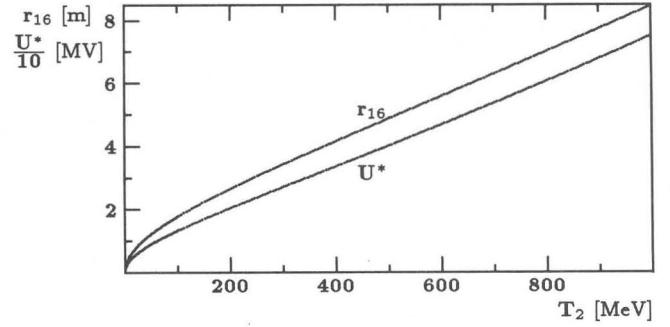


Fig. 10. The extraction radius r_{16} and the accelerating voltage U^* versus the extraction energy T_2

Figure 10 shows r_{16} and U^* versus the final energy T_2 . Both curves are almost straight lines for $T_2 > 200$ MeV. Due to Eq.10 the number of sectors and the number of cavities $N_{cav} = N_{sec} - 1$ depend linearly on T_2 . In table 1 some data of three systems are summarized, each consisting of two Tritron ring, with the final energy 500 MeV, 750 MeV and 1000 MeV. r_{in}^I and r_{in}^{II} indicate the injection radius of the first resp. the second ring, r_{ex}^{II} the extraction radius of the second ring. The number of sectors is assumed to be 16, of course detailed beam dynamic calculations may lead to somewhat smaller numbers. The maximum power, which has to be transmitted to a 10 mA proton beam per cavity, is less than 190 kW. Present input couplers for superconducting cavities are operated at up to $\simeq 200$ kW. The limiting effects for the beam

Table 1. Some data of 2-ring systems for 500 MeV, 750 MeV and 1000 MeV

	a)	b)	c)
$T(r_{ex}^{II})$ [MeV]	500	750	1000
$T(r_{in}^{II})$	151	271	393
$T(r_{in}^I)$	33	101	180
r_{ex}^{II} [cm]	486	663	845
r_{in}^{II}	326	503	685
r_{in}^I	166	343	525
$U^*(r_{ex}^{II})$ [MV]	40	57	75
$U^*(r_{in}^{II})$	12	16	20
$U^*(r_{in}^I)$	4	7	9
N_{sec}^I	16	16	16
N_{sec}^{II}	22	32	42
N_{cav}	21 + 7	31 + 9	41 + 15
N_{mag}	608	768	928
ν [MHz]	7.4	6	4.9
$h = \nu_{rf}/\nu_o$	12	15	18

current are similar to those known from proton storage rings. The beam creates fields, the space charge fields and those from image currents on the beam tube walls, which act back on the beam itself. All related effects depend mainly on the longitudinal and transverse coupling

impedances. Pure inductive and capacitive impedances cause real, intensity dependent shifts of the betatron and synchrotron oscillation numbers, and some change of the bunch dimensions. A resistive impedance causes imaginary frequency shifts $\Delta\omega$ and eventually instabilities, with the time constant of growth given by $\tau = -1/\Im(\Delta\omega)$. In the Tritron the beam runs either in a copper tube inside the channel magnets or in a cavity gap. The influence of the slits between the tubes and the cutoff bores of the cavities is assumed to be negligible.

The resistive wall effect of the copper tubes is expected to be much less compared to that of stainless steel vacuum chambers normally used in storage rings. The surface resistance of cold copper at 500 MHz for example is about 40 times less than that of stainless steel at room temperature (anomalous skin effect). Furthermore each individual bunch traverses one ring within $16/\nu_0 \simeq 3 \cdot 10^{-6}$ sec. This limits the time for the development of an instability. The reactive part of the impedance in the Tritron is mainly determined by the space charge effect. It decreases strongly with increasing particle energy. It can be overcome by choosing the injection energy sufficiently high. In addition, in the Tritron rather large shifts of the betatron oscillation numbers are admissible due to the insensibility to resonance problems. Longitudinally the high accelerating voltage per turn causes unusual high synchrotron oscillation numbers, so that rather large shifts are admissible here also.

The superconducting cavities are traversed by 16 bunches in parallel, radially distributed along a large range. So the excitation of higher order modes by the beam has to be expected. Some special features of the Tritron cavities may be helpful to overcome these problems. First the cavities are single cells, resulting in a simple line spectrum without broad passbands. Thus there will be a certain chance to detune the cavity with respect to the frequency of a special higher order mode, which may be excited by the beam. Secondly, the quality factor of all modes with surface currents crossing the horizontal plane of symmetry are reduced due to the poor flat rf-joint. Finally, the cavity volume is accessible from all sides to install higher order mode couplers in an effective manner, avoiding trapped modes as in some multicell cavities. The interaction of several parallel high intensity bunches with a superconducting Tritron cavity can be investigated experimentally by triggered electron pulses through the beam holes, theoretically by means of computer codes. So far various storage rings with superconducting multicell cavities operate stably with beams above 10 mA. In HERA at DESY a current of 60 mA is envisaged for the near future.

6. ACKNOWLEDGEMENTS

Thanks are given to all members of the Tritron group, especially to M.Arnold, A.Cazan, G.Hinderer, R.Kratz, and P.Schütz, who have made important contributions to this work. Sincere thanks also to V.P.Dmitrievsky and S.B.Vorozhtsov from JINR /

Dubna for fruitful discussions during many years.

This work was funded by the German Federal Minister for Research and Technology (BMFT) under the contract number 06 TM 189.

7. REFERENCES

- 1) Trinks, U., Assmann, W., Hinderer, G., "The Tritron: A superconducting separated-orbit cyclotron", Nucl. Instr. Meth., **A244**, 273 (1986),
- 2) Hinderer, G. and Trinks, U., "Beam dynamics in the Tritron", Nucl. Instr. Meth., **A244**, 283 (1986),
- 3) Russell, F.M., "A fixed-frequency, fixed-field, high-energy accelerator", Nucl. Instr. Meth. **23**, 229 (1963),
- 4) Martin, J.A., "The separated-orbit cyclotron", IEEE Trans. Nucl. Sci. **NS-13**, 288 (1966),
- 5) Trinks, U., "Longitudinal particle dynamics in the Tritron", Nucl. Instr. Meth. **A306**, 27 (1991),
- 6) Hinderer, G., Rieß, C., Trinks, U., "Transverse beam dynamics and coupling effects in the Tritron", Nucl. Instr. Meth. (1992),
- 7) Kratz, R., Hinderer, G., Junger, J., Labedzki, J., Trinks, U., "The superconducting Tritron magnets", IEEE Part. Accel. Conf., May 6-9, 1991, San Francisco, 2254,
- 8) Schütz, P., Grundey, T., Labedzki, J., Trinks, U., "The superconducting cavities for the Tritron", IEEE Part. Accel. Conf., May 6-9, 1991, San Francisco, 2450,
- 9) Grundey, T., Labedzki, J., Schütz, P., Trinks, U., "The superconducting accelerating cavities for the Tritron", Nucl. Instr. Meth. **A306**, 21 (1991),
- 10) Aab, V., et al., "The superconducting 130 MeV electron accelerator at Darmstadt", Proc. European Part. Accel. Conf., 1988, Rome, 335,
- 11) Dietl, L., Trinks, U., "The surface resistance of a superconducting lead-tin alloy", Nucl. Instr. Meth. **A284**, 293 (1989),
- 12) Hinderer, G., Leu, M., "The beam matching for the tandem-Tritron accelerator system", Nucl. Instr. Meth. **A287**, 287 (1990),
- 13) Rohrer, L., Schnitter, H., Walchshäusl, B., "The tandem Tritron control system", Nucl. Instr. Meth. **A287**, 170 (1990),
- 14) Joho, W., "High intensity problems in cyclotrons", 9th Int. Cycl. Conf., Caen 1981, 337